Astron. Astrophys. 320, 325–332 (1997)

ASTRONOMY
AND
ASTROPHYSICS

Intermediate teeth in pulsed jets: a motivation for high-resolution observations

Michael D. Smith[1], **Gerhard Suttner**[1], **and Hans Zinnecker**[2]

[1]Astronomisches Institut der Universität Würzburg, Am Hubland, D-97074 Würzburg, Germany
[2]Astrophysikalisches Institut Potsdam, An der Sternwarte 16, D-14482 Potsdam, Germany
(smith, suttner@astro.uni-wuerzburg.de, hzinnecker@aip.de)

Received 26 February 1996 / Accepted 12 September 1996

Abstract. Supersonic jets often contain a series of knots which can be interpreted as arising from a pulsating energy source. The pulsation model is here examined for uniquely-identifying signatures. Formulae are presented for the number, intensity and distribution of knots.

Our numerical and analytical calculations confirm that the classical sawtooth velocity structure contains intermediate teeth. The intermediate teeth are shown to possess high-velocity gradients, between 1.6 to 3 times the sawtooth gradient for models ranging between adiabatic and isothermal. Both sets of teeth weaken with distance with only positive gradients allowed. The leading shock of one pulse can catch up with the reflected shock of the pulse ahead. Then, the intermediate teeth form a new weaker sawtooth structure, with about half the original jump, upon which new teeth are weaned. This gives rise to a relatively long-period beat-type pattern. The associated velocity and spatial structures should soon be observable in protostellar jets.

Key words: hydrodynamics – shock waves – ISM: jets and outflows – galaxies: jets

1. Introduction

Compact astrophysical objects can undergo a phase in which enormous amounts of gas are ejected within narrow supersonic jets. These outflows are usually not smooth but contain a number of bright knots. Recent breath-taking observations include the extragalactic 3C 273 synchrotron-radiation jet (Bahcall et al 1995) and the protostellar HH 212 molecular-hydrogen jets (Zinnecker et al). The interpretation of the knots remains unclear and provides the motivation for this study.

Regular outbursts of activity should produce pulsed jets (Rees 1979). Hydrodynamic pulses turn into sharp velocity decreases (shock waves), separated by zones of gradual partial recovery - a weakening sawtooth pattern along the jet (Raga et al 1990). Here we study the velocity patterns generated. In particular we wish to understand the nature of the intermediate modes uncovered by Stone & Norman (1993). These modes can rapidly dominate the velocity structure and may provide the most confident means of identifying the cause of knotty jets and confirming the validity of the hydrodynamical approach. Unfortunately, no physical analysis of this phenomenon has been attempted. We amend this neglect here by developing a theoretical framework from which quantitative predictions can be extracted.

There is now much evidence that pulsed outflows do occur, including proper motions of distinct knots and highly-symmetric bipolar structures (see Raga et al 1990, Ray 1996), although it is clear that the pulsation mechanism is only one cause of jet structure (e.g. Eislöffel & Mundt 1994). In particular, the Kelvin-Helmholtz instability operates across the jet boundary. The pinching mode of this fluid-dynamic instability can also lead to a series of knots (e.g. Ferrari et al 1983). Furthermore, wiggles in the jet also have contrasting explanations: ejection variations (e.g. precession) and propagation problems (helical modes of the Kelvin-Helmholtz instability) have been investigated (see Loken et al 1995).

Models for the development and progression of shocks down a jet have already investigated the saw-tooth velocity structure to make testable quantitative predictions. It has generally been presumed that shocked material squirts laterally out of the jet (or can be considered as compressed into a layer of negligible observational consequence) (Raga & Kofman 1992, Raga et al 1993). This is supported by partial (i.e. symmetric single knot) simulations (Falle & Raga 1993). Although this is indeed true, theoretical considerations (see Sect. 5.1) and full high-resolution numerical simulations reveal that another process determines the knot and shock properties: while expansion transverse to the jet (i.e. through the walls) is present, the parallel expansion is more important. Both one and two dimensional runs have uncovered the gradual growth of *intermediate teeth*: a pulse consists of two separating shocks which sandwich the higher-pressure shocked gas (Hartigan & Raymond 1993; Stone

Send offprint requests to: M.D. Smith

& Norman 1993). Moreover, a steep velocity gradient on the jet axis is present across this sandwich. Can this gradient be observed through modern spectroscopic techniques? We here wish to determine (1) the growth rate of the size of a knot, (2) the growth of the velocity gradient across the knot and (3) the evolution of the whole pulsed structure. In this context, upcoming high-resolution infrared and optical observations of the jets from young stellar objects provide strong motivation (e.g. HST infrared and VLT optical).

The model presented here is based on new one-dimensional numerical simulations. The hydrocode is Eulerian, time-explicit and spatially second-order (see Ziegler et al 1996 for a full description). It follows the Stone & Norman (1992) description and is being adapted to simulate molecular outflows; two-dimensional results confirm the existence of intermediate teeth in molecular jets (Suttner et al 1996). Here, sinusoidal velocity perturbations on uniform jets propagating into a uniform environment are studied. Both isothermal and adiabatic models are considered. First we display the numerical results which exhibit the rules used in the analytical model. The major point is that, unless extremely large disturbances are encountered, it is possible to model a train of knots (including their interactions) by considering the evolution of a single tooth contained within a segment bounded by identical segments.

2. Numerical examples

One-dimensional time-dependent simulations of an ideal gas with specific heat ratios in the range 1.01 to 5/3, to cover both adiabatic and quasi-isothermal conditions, are displayed in Figs. 1 & 2. A fluid is injected from one end of the grid (the nozzle end) with a speed of 100 km s^{-1}, temperature 100 K and molecular weight 2, corresponding to a Mach number of M = $155/\sqrt{\gamma}$. The initial jet density is 10^5 cm^{-3}, 10 times higher than the ambient stationary gas, which has an initial temperature of 10 K. Note that these conditions only approximate an astrophysical situation. The first goal is to understand the dynamics, rather than determine the influence of factors such as ionisation, magnetic energy and cooling.

Sinusoidal perturbations of amplitude 10 km s^{-1} and period 100 years are superimposed onto the injected gas. Results are shown in Fig. 1 for the velocity and in Fig. 2 for the density. These results correspond to a late time in the calculation and are typical in the sense that each pulse evolves in the same manner as it moves along the jet. Thus the train of pulses at one instant demonstrates the development of a single pulse over it's propagation lifetime (until it approaches the ambient medium). Crucial factors displayed here, consistent with previous simulations, are as follows.

(1) After about one wavelength from the nozzle, the wave has steepened into a sawtooth structure. The double shock structure is spatially resolved after several wavelengths. A sharp peak is then produced in the density profile. This density peak defines the knot and separates the forward shock from the reverse shock (although both shocks move downstream). (Note that a train of single forward shocks propagating down the jet would, in general, be generated by a monotonically increasing energy source rather than pulsations.)

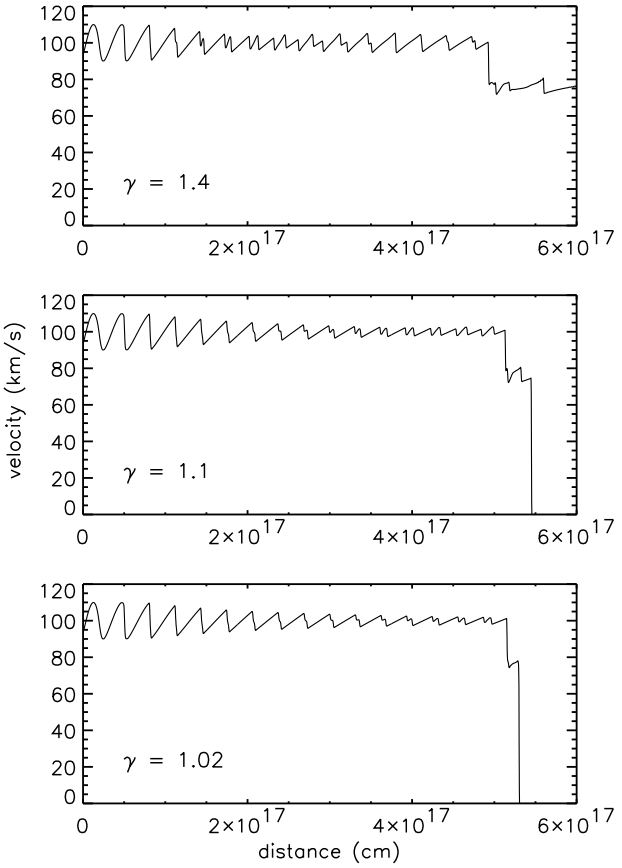

Fig. 1. One-dimensional pulsed jets. The velocity patterns for three specific heat ratios are shown. The jets (10^5 cm^{-3}, ten times the ambient density) propagate over 5 10^{17} cm at the time 2159 years of these snapshots. Note how the pulse development depends on γ.

(2) The two shocks separate at a rate which depends crucially on the specific heat ratio. Lower γ flows take longer to develop their intermediate teeth. The alternative model has separating shock pairs due to a balance between the mass entering the tooth from the jet and the mass lost through the sides (Biro and Raga 1994). The reason why this balance is not observed in the full simulations will be elucidated by the analytical model in Sect. 5.

(3) A dense knot is formed between the shock pairs. The density contrast is greater for the lower γ flow.

(4) A pulse tires i.e. the amplitude becomes smaller as more material is swept up into the knots.

(5) The velocity gradient between the shock pairs is much steeper than the velocity gradient between the pulses. The appearance of the new teeth must only for numerical reasons be spread out over a large number of zones to simulate the drastic changes in speed.

(6) As a pulse tires, the velocity change across an intermediate tooth continues to rise even though its gradient also

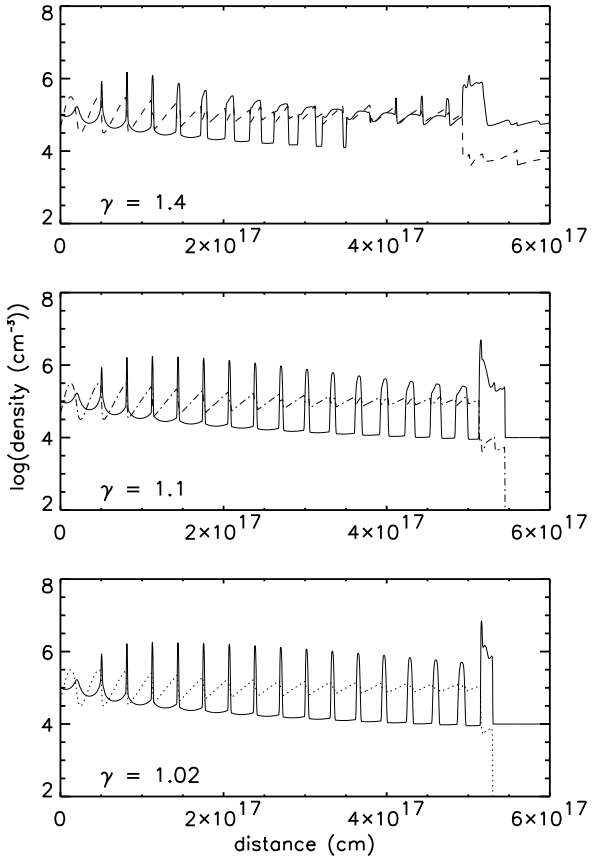

Fig. 2. The density structure for the three jet models displayed in Fig. 1. The velocity patterns (dashed lines) from Fig. 1 are superimposed in arbitrary units. Note that the inter-knot density gradually falls due to the expansion, causing the knots to tire, until the second-phase (knot-knot interactions) begins (here, this phase is reached only for the $\gamma = 1.4$ case where three second phase knots can be seen between $4 - 5\,10^{17}$ cm).

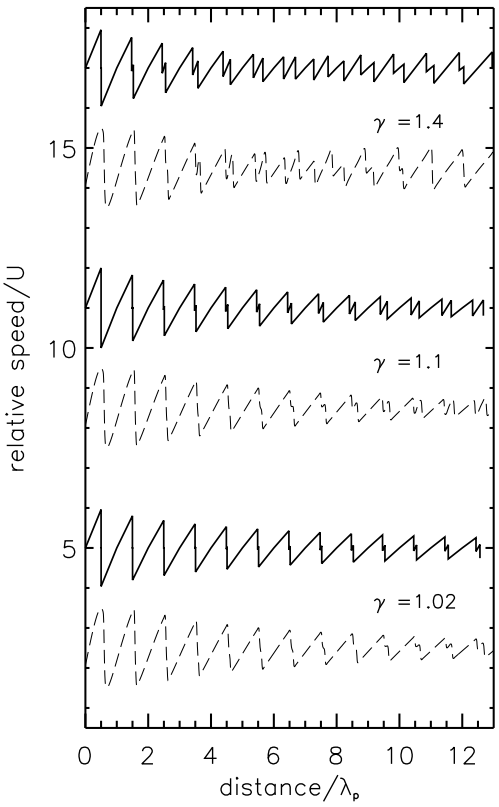

Fig. 3. A comparison of the analytically-predicted velocity profiles (solid lines) with the numerical results from Fig. 1 (dashed curves) for three adiabatic flows. The first 13 wavelengths are displayed where $\lambda_p = 3.16\,10^{16}$ cm (howver the first unsteepened wave in the numerical results has been extracted). Arbitrary speeds have been added purely for display purposes. Note that the fast-evolution of the $\gamma = 1.4$ case is predicted but the analysis becomes inaccurate as the knots (i.e. the shock spacing) becomes large.

decreases. Thus the intermediate teeth end up dominating the velocity structure for all γ.

(7) The density between the knots falls as it is swept up into the knots. It rapidly becomes uniform through the expansion. Each pulse possesses high symmetry i.e 180° rotational symmetry about the center of the intermediate tooth, as shown in Fig. 3.

Can these behavioural patterns be quantified?

3. Analytical foundations

3.1. The sawtooth framework

The velocity structure of a pulsed jet is controlled by a one-dimensional thrust-pressure balance (Sect. 5.1). That is, at any moment, the accumulated gas in the knot and the gas just compressed by the shocks are in approximate thermal pressure equilibrium. This fixes the shock strength and position. This simple model is developed here and proves to be extremely accurate when compared to both 1-D (Fig. 3) and 2-D (Fig. 4) simulations.

The nature of a pulse must be greatly simplified if we hope to extract analytical results. We take advantage of the symmetry to consider only the *left half* of the pulse shown in Fig. 5. We shall also first consider the case of a high Mach number flow so that we can take the strong shock limit in which the compression and pressure jump,

$$\frac{\rho_2}{\rho_1} = \frac{\gamma + 1}{\gamma - 1 + 2/M_1^2} \tag{1}$$

$$\frac{p_2}{p_1} = \frac{2\gamma M_1^2 - (\gamma - 1)}{\gamma + 1} \tag{2}$$

as prescribed by the Rankine-Hugoniot relations (e.g. Priest 1982), are reduced to $(\gamma+1)/(\gamma-1)$ and $2\gamma M_1^2/(\gamma+1)$, respectively. Here M_1 is the shock Mach number. Low Mach numbers will only be considered in the alternative isothermal case studied below.

We examine the hydrodynamic evolution of the pulse shown in Fig. 5 given that the speed V(t) = 0 is fixed at x = 0 and x = D.

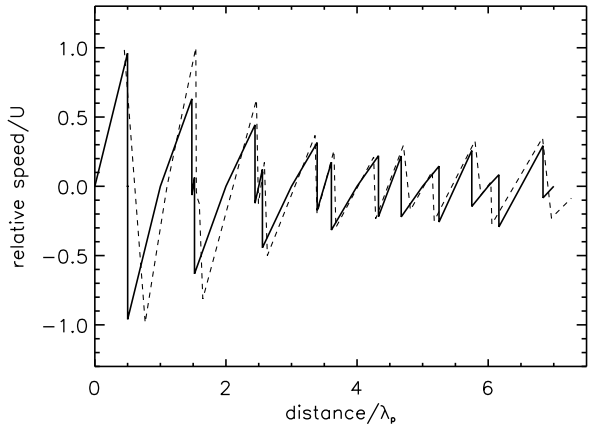

Fig. 4. An analytic solution for an isothermal jet (thick line) taking the parameters of the Stone & Norman (1993) 2D-C simulation, the results of which (dashed line) are in superb agreement given the different approximations involved. The velocity amplitude is A = 0.25, $M_o = 5$, $\lambda_p = 1.65\,10^{16}$cm and $v_j = 235$km s^{-1}. The distance has been shifted by $+0.45\lambda_p$ for the numerical result, implying that the initial steepening and appearance of the teeth are very rapid.

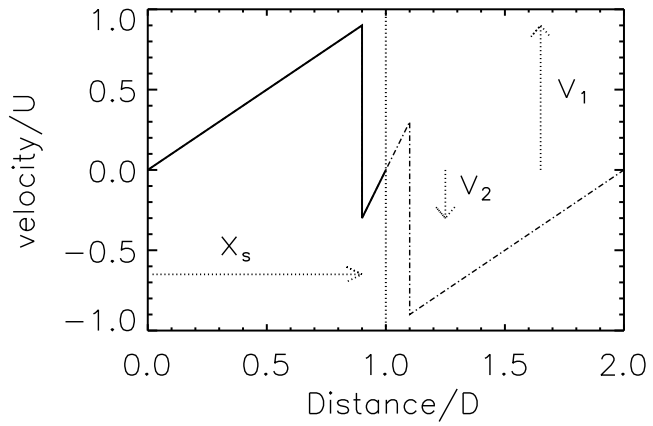

Fig. 5. Isolation of a pulse and the reduction of the flow problem employing the symmetries observed in the slowly-evolving pulses displayed in figs. 1 and 2. Note the pulse wavelength is $\lambda_p = 2D$.

The problem is completely defined given the pulse velocity-amplitude U. Thus at t = 0, V = UX/D for $0 \leq X < D$. This is the classical saw-tooth structure. We redefine the time in units of D/U, and put x = X/D and v = V/U.

A single shock (subscript s) occurs in the half-pulse considered. In the inter-pulse region (i.e. the unshocked jet), the density is taken as a function only of time (see point 6 above). This will hold quite generally for smoothly varying perturbations, along with the sawtooth velocity profile, due to the continued expansion of the unshocked gas. The Navier-Stokes equation for negligible force and pressure gradient (Burger's equation)

$$\frac{dv}{dt} + v\frac{dv}{dx} = 0 \tag{3}$$

and the mass conservation equation yield the inter-pulse solution (for $x < x_s$):

$$\rho(t) = \rho_o/(1+t) \tag{4}$$

$$v = x/(1+t). \tag{5}$$

Note that at t = 0, the compression yields $v_s = -(\gamma-1)/2$, (in units of U), so that the shock reduces the speed from 1 to zero. The post-shock pressure is then $2(1-v_s)^2/(\gamma+1) = (\gamma+1)\rho_o U^2/2$ (in units of $\rho_o U^2$), on using equation (2). The sound speed in the shocked gas is $c_s = \sqrt{\left[\gamma(\gamma-1)/2\right]}$

3.2. The hydrostatic-dynamic equilibrium

We shall require the position and strength of the shock to be determined by the balance between the pressure of the gas instantaneously passing through the shock (i.e. the supersonic thrust) and the thermal pressure of the expanding-layer of subsonic post-shock gas. The pre-shock speed is $v_1 = x_s/(1+t)$ which yields $dv_1/dt = v_1(v_s - v_1)/x_s$. The thrust is the post-shock pressure (equation 2). Thus we have $p_s = 2\rho(v_1 - v_s)^2/(\gamma+1)$. This gives a changing thrust on the knot of:

$$\frac{dp}{dt} = -p\left[\frac{3v_1}{x_s} + \frac{2\dot{v}_s}{v_1 - v_s}\right]. \tag{6}$$

The pressure decrease must be balanced by the adiabatic expansion of the already-present fluid in the knot, pV^γ = constant

$$\frac{p(t+dt)}{p(t)} = \left[\frac{1-x_f(t)}{1-x_f(t+dt)}\right]^\gamma \tag{7}$$

where x_f can be any fluid element in the post-shock flow. We thus take $dx_f/dt = v_2$, as the flow speed immediately behind the shock to yield

$$\frac{\gamma v_2}{1-x_s} = -\left[\frac{3v_1}{x_s} + \frac{2\dot{v}_s}{v_1 - v_s}\right] \tag{8}$$

where shock compression requires $(v_2 - v_s)/(v_1 - v_s) = (\gamma-1)/(\gamma+1)$. On substitution, we reduce the problem to a single differential equation for x_s:

$$\frac{2\dot{v}_s(1+t)(1-x_s)}{x_s - v_s(1+t)} + 3\frac{1-x_s}{1+t} +$$

$$\frac{\gamma}{\gamma+1}\left[2v_s + \frac{x_s(\gamma-1)}{1+t}\right] = 0. \tag{9}$$

This equation is easy to solve numerically. As shown in Fig. 6, the teeth develop with all the properties noted in Sect. 2.

Taking a time sequence of solutions, each separated by a time $2D/v_j$ and appending them in space yields a jet snapshot. The agreement of this analysis (Fig. 3) with the numerical results (Fig. 1) is excellent.

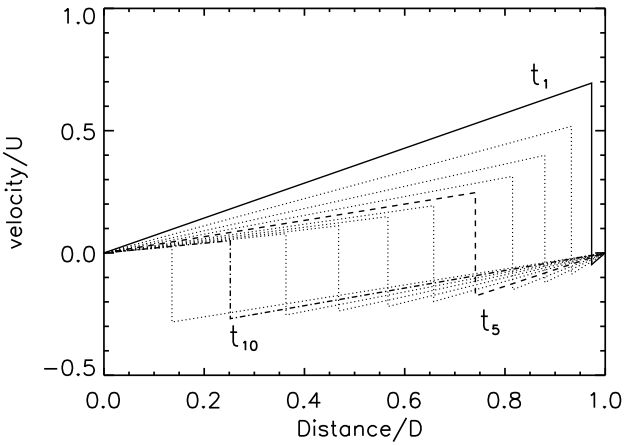

Fig. 6. The time sequence for the pulse velocity structure with $\gamma = 1.1$ obtained via the analysis. Each tooth is separated by a time 0.2 D/U, from the solid line (t_1 = 0.2 D/U), through the dash (t_5 = D/U) to the dot-dashed line at t_{10} = 2D/U. Note that the sawtooth amplitude, shock jump and velocity gradients all decrease with time.

3.3. Isothermal pulses

Equation (7) above holds for the isothermal case. We only need to adjust the expression for v_2 to that appropriate for the compression $M_p^2 = (v_1 - v_s)^2/c_s^2$ across an isothermal shock. This yields $v_2 = v_s + 1/\left[M_o^2(v_1 - v_s)\right]$ where M_o is defined as U/c, c being the sound speed. In this case the initial shock speed is $v_s(0) = -\left[\sqrt{(1 + 4/M_o^2)} - 1\right]/2$ (on setting $v_2 = 0$). Results of the integration are shown in Fig. 4. Excellent agreement is again obtained with these two-dimensional simulations.

Hence we can now use this analysis to quantify the teeth characteristics and determine our ability to observe them.

4. The velocity gradients

Some illuminating analytical results are derivable for the velocity gradients in the intermediate teeth. As the shocks begin to separate, the pressure balance argument and the neglect of mass loss through the walls are both extremely accurate approximations since the shocked layer is thin. The initial acceleration and velocity gradients are thus independent of the assumptions. When the shocks are far apart, the model requires that no significant pressure gradient forms between them, a condition consistent with the numerical findings.

The velocity gradient which separates the shock pairs may be directly observable at high spatial resolution or indirectly through double-humped or broad line profiles.

The gradient is derived by first finding the initial shock acceleration, a quantity constrained by the model. Putting $v_s = -(\gamma - 1)/2 + \dot{v}_s\delta t$ and $v_1 = 1 - \delta t(\gamma + 1)/2$ at $t = \delta t$ into Eqn. (8) yields the initial shock acceleration for any adiabatic high M_o pulse:

$$\dot{v}_o = -\frac{(\gamma^2 - 1)(3 - \gamma)}{4(2\gamma - 1)} \tag{10}$$

and for the isothermal shock of any Mach number:

$$\dot{v}_o = -4\frac{1 + \sqrt{(1 + 4/M_o^2)}}{8 + M_o^2\left[1 + \sqrt{(1 + 4/M_o^2)}\right]}. \tag{11}$$

These values were used as part of the initial conditions in the numerical solutions of this section. Substitution back into Eqn. (8) yields the fluid velocity gradients within the pulse, $\nabla v_f = -v_2/(1 - x_s)$:

$$\nabla v_f = \frac{\gamma + 2}{2\gamma - 1} \tag{12}$$

and

$$\nabla v_f = 3 - \frac{16}{M_o^2\left[1 + \sqrt{(1 + 4/M_o^2)}\right] + 8}. \tag{13}$$

These both take the maximum gradient of 3 (units of U/D, the initial sawtooth gradient) in the limit of an isothermal high Mach number pulse. For $\gamma = 5/3$, 10/7 and 7/5, three adiabatic cases of importance, the gradients are 11/7, 24/13 and 17/9, respectively, i.e. in the range 1.5 to 2.

In the isothermal case, the gradients can be large even though the original flows were completely subsonic. For example, for $M_o = 1/\sqrt{2}$, the gradient is 7/5. However, for subsonic flows, the initial development of a sawtooth velocity structure appears to lead to a sawtooth pressure structure, restricting a pulse to a single shock.

We conclude here that the steepest gradients occur in high Mach number strongly-cooling flows i.e. in the conditions appropriate to protostellar jets.

5. Hydrodynamical implications

5.1. The flow pattern

The velocity structure of a pulsed jet is controlled by the one-dimensional thrust-pressure balance. This is supported by the following arguments.

- Our analysis is based on full one and two dimensional simulations of velocity-pulsed jets. These simulations show that intermediate teeth grow and are not quenched by sideways mass escape. In contrast, the work of Falle & Raga (1993) demonstrates the existence of a steady state in which gas escapes laterally at the same rate as it passes through the shocks. This result does not apply here since the gas was injected at a steady rate by Falle & Raga, and thus did not simulate the crucial pulse-tiring effect. In pulsed jets, the jet thrust (between pulses) rapidly decreases causing a high expansion along the jet axis. Sideways expansion, in which material spills out of the jet, while not inhibited, is slow at reducing the knot pressure. This is quantified below.
- The initial flow near the knots is one-dimensional since they are very thin disks. That is, the initial mass-loss is negligible and the formulae presented in Sect. 4 for the initial velocity gradients should be very accurate. *The strong gradients and high axial expansion are thus formed early and continue to dominate the flow pattern at later times.*

– One and two dimensional numerical results demonstrate qualitatively identical flow patterns which prompt the need for a single interpretation. The model developed here is consistent with both one-dimensional (Fig. 3) and two-dimensional (Fig. 4) simulated flows.
– Taking into account the mass lost through the jet walls, but not the shock thrust, Biro and Raga (1994) built a model which failed to predict the size of the growing knots, which was about three times smaller than seen in their numerical experiments (note also that the quoted (numerical) jet radius is in fact the jet diameter, increasing the discrepancy).

The above arguments can be quantified as follows. Firstly, it can be shown that the mass outflow through the knot walls is large: $2\epsilon\pi(1-\mathrm{x_s})\rho_\mathrm{k}\mathrm{r_j}\mathrm{Lc_s}$ where $\mathrm{r_j}$ is the jet radius and ϵc_s is the representative transverse expansion speed. The rate at which mass enters the knot is $\pi(\mathrm{v_1}-\mathrm{v_s})\rho\mathrm{r_j^2U}$. This yields the ratio of mass outflow to inflow of $4\epsilon\mathrm{M_1}(1-\mathrm{x_s})\mathrm{L/r_j}$ in the isothermal case. This clearly is small only in the early phase of the knot formation. However, a balance is never achieved between the inflow and outflow because the lateral expansion rapidly increases: given the velocity gradient in the knot of $\sim 3(1-x_s)U$, the lateral to transverse speed is $\mathrm{v_2/c_s}\sim 3(1-\mathrm{x_s})\mathrm{U/c_s}$. Hence, apart from the early phase, the knot properties are controlled by the strong transverse expansion.

5.2. Second-phase knots

What results when one tooth catches up with another? In principle, the pulses remain separated by one wavelength. However the intermediate teeth travel between pulses and thus interact. This is seen most clearly in the $\gamma = 7/5$ case presented here (see also Stone and Norman 1993). The result is a second series of intermediate teeth. The original teeth have disappeared, having been replaced by the intermediate set.

This second phase involves weaker shocks. Whereas the velocity jump across the first sawtooth to appear was 2U, the new teeth appear on a sawtooth structure of amplitude ~ 0.82U, 0.60U & 0.36U for the adiabatic jets $\gamma = 1.4$, 1.1 & 1.02, and $\sim$ 1.06U, 0.68U & 0.30U for isothermal jets with M = 2, 5 & 20. Hence, the teeth interactions may have the greatest consequence for non-cooling or low Mach number flows.

The new teeth have different properties. They occur within denser gas which has already been shocked once. Hence this gas is hotter (despite some cooling through the adiabatic expansion). High asymmetries are now generally unavoidable since the interaction region can no longer be isolated to a small section of the jet.

The knot locations become 'reversed'. The new density (and temperature) peaks now occur in the periodic location (i.e. the phase) where the density troughs were located (see Fig. 2). If one attempts to follow the centroids of the density peaks for the train of pulses, one finds that a jump of half a period occurs. Hence, although the flow begins to appear masticulated (especially where large-amplitude pulses are involved i.e Stone & Norman 1993), observable signatures are still predicted.

6. A search for observable properties

6.1. Spatial distribution

Double-shock structures are predicted. But can the twin-shocks be spatially resolved? We can estimate this separation distance, $\mathrm{L} = 2(1-\mathrm{x_s})\mathrm{D}$, as a function of distance along the jet, $\mathrm{z_j}$ from the formulae of Sect. 4. To ease the connection to the observations we revert to absolute values. We employ the jet speed $\mathrm{v_j} = \mathrm{z_j/t}$ where t is the time elapsed for a particular pulse since it appeared as a sharp sawtooth structure. The pulse velocity amplitude is $\mathrm{U} = \mathrm{Av_j}$ where A is the relative amplitude as employed by Stone & Norman (1993). We also have the pulse period P and wavelength $\lambda_\mathrm{p} = 2\mathrm{D} = \mathrm{Pv_j}$ and *jet* Mach number $\mathrm{M_j} = \mathrm{v_j/c_s} = \mathrm{M_o/A}$.

We take here the high-M_o isothermal case in which the initial shock acceleration is $\dot{\mathrm{v}}_\mathrm{o} \sim -4\mathrm{U}^2/\mathrm{DM_o^2}$, from equation (6). Note that the initial shock speed is relatively low but grows through the acceleration. The acceleration generally changes slowly, by a factor $\sim 0.5-2.0$ after the shocks are separted by a distance D. Hence we take a constant acceleration and employ a function $\eta(M_o)$ which is a weak function of the variables i.e we write $\mathrm{L} = -\eta\dot{\mathrm{v}}_\mathrm{o}\mathrm{t}^2$ which can be rewritten in terms of the fraction of the jet occupied by the knots (on replacing t by $\mathrm{z_j/v_j}$):

$$\frac{L}{\lambda_p} = \frac{8\eta N^2}{M_j^2}, \tag{14}$$

where $\mathrm{N} = \mathrm{z_j}/\lambda_\mathrm{p}$ is the number (and fraction thereof) of the pulse from the sawtooth-jet origin.

The number of knots in a string before shocks interact (i.e. the first phase) is thus restricted to $\mathrm{N_a}\sim \mathrm{M_j}/(\sqrt{(8\eta)})$ in a time $\mathrm{t_a} = (\lambda_\mathrm{p}/\mathrm{U})\mathrm{M_o}/\sqrt{(8\eta)}$. The number is *simply proportional to the jet Mach number*, independent of the pulse properties. Thus an atomic isothermal jet of speed 300 km s^{-1} with a sound speed of 14 km s^{-1} would begin with only a few knots spaced by λ_p before degenerating into an uneven sequence with an average spacing of $\lambda_p/2$.

6.2. The observable number of knots

The practical question of spatial resolvability depends on the observability of the knots. The pulses fade rapidly, here simply interpreting brightness in relation to the energy flux through the shock front. The high-M_o case illustrates the outcome as follows. The energy flux is $\dot{E} = \rho(v_1 - v_s)^3/2$:

$$\dot{E} = \rho_o U^3 \left[1 - \frac{\eta\dot{v}_o t^2}{\lambda_p}\right]\left[1 + \frac{2Ut}{\lambda_p}\right]^{-4}, \tag{15}$$

on substitution from Sect. 3. Thus by knot $\mathrm{N_k}$, just before the pulse shocks interact, the power has fallen by a factor of $\sim \mathrm{M_o^4}/32$: high-speed pulses fade extremely fast.

How many pulses could we then reasonably expect to observe? After a pulse time $\mathrm{t_{obs}} = \lambda_\mathrm{p}/(2\mathrm{U})$, the pulse flux has

fallen by a factor of 16. Taking this to correspond to the instruments's dynamic range, the number of observable knots is then $v_j t_{obs}/\lambda_p$ or

$$N_{obs} \sim \frac{1}{2A} \tag{16}$$

where $\eta = 1$ has been taken since the acceleration is constant in this early phase. Hence *the number of observable knots in the initial sequence is inversely proportional to the pulse amplitude*.

The knot size is just $L_{obs} \sim 2\lambda_p/M_o^2$ (on using equation (14)). Thus, a high dynamic-range in combination with high spatial resolution is necessary. Hot jets (i.e. with a high sound speed) would ease the resolution problem.

6.3. Knot renovation/rejuvenation

A brightening of the knots will take place at a distance of $\sim (N_a + 1)\lambda_p$, where the pulse shocks collide. The first shocks in this new sequence will have speed $\sim \sqrt{(-\dot{v}_o \lambda_p)}$ (i.e. through constant acceleration over a distance $\lambda_p/2$. The density in the knots has fallen after the shock compression through the expansion. The expansion tends to smooth out the density profile so that the density upstream of the shocks (which was downstream of the shocks up to this point) is approximately constant and, therefore, just as the two shocks interact (i.e. an elastic collision, or pure reflection, with no transmission when of equal strength as taken here), equal to the initial density ρ_o.

The high-M_o case yields a shock energy flux $(\rho_o U^3)\left[16\sqrt{2}/M_o^3\right]$. For example the flux has fallen by a factor of 50 from the initial knot for a M_o of 10. However, the flux has risen from the preceding knot, number N_k, by a factor $M_o/\sqrt{2}$, or a factor of 7. Thus a jet can appear to be switched on for a second time.

6.4. Velocity resolution

Are the velocity jumps observable? We shall here suppose that a jet is quite close to the line of sight. Other orientations would reduce the spectral width of line emission appropriately. Moreover, only the emission from the jet is examined; external shocks which may flank the jet knots are neglected. Given these restrictions, we still may ask the general question: what is the maximum velocity width for line emission from the knots? This question is relevant when the radiated energy is dominated by the cooled compressed gas rather than the hot gas, such as for molecular hydrogen infrared emission from hydrodynamic shocks. Then, the infrared emission is generated mainly in the compressed and cooled (down to a few thousand Kelvin) gas. For a spatially-unresolved knot, the velocity increases from $-v_2 U$ to $+v_2 U$, for a full width of $2v_2 U$ where v_2 is given in Sect. 3.3. This velocity width increases as the knot grows.

If the number of observable knots is as described in Sect. 6.2, then it is straightforward to show that at time t_{obs}, $2v_2 U \sim 4/M_o^2$, in the high-M_o constant-acceleration estimate. This is clearly very small. Once again a low M_o flow without sacrificing energy flux (i.e. a jet with high sound speed) would generally provide the best identifying conditions.

The highest knot velocity jump occurs just before the pulse shocks collide after a time $t_a = M_o\lambda_p/(2\sqrt{(2\eta)}U)$. This yields $v_{max} = 4\sqrt{(2\eta)}\left[1 - 1/(8\eta)\right]/M_o$. Thus lines can be very wide due to the knot expansions e.g. a width of $\sim$ U/2 is predicted for $M_o = 10$.

The maximum overall fluid velocity width is, however, not always given by twice the post-shock speed, $2v_2$. The unshocked gas as well as the gas within the shock front itself may well dominate even in molecular jets. The sawtooth amplitude is thus the quantity that may be observable. Due to the high-speed knot expansion the total sawtooth amplitude decreases faster than previous estimates. Here it is given by $v_{saw} = 2Uv_1(x_s) = 2x_s U/(D + tU)$. Substitution yields

$$v_{saw} = (1 - \frac{8\eta}{M_o^2}\left[\frac{Ut}{\lambda_p}\right]^2 /(1 + 2\left[\frac{Ut}{\lambda_p}\right]) \tag{17}$$

This remains, however, higher than v_{max} while the knot is narrow. Once the knot size is of order of the wavelength, the velocities become comparable (see Figs. 3 & 6).

7. Conclusions

We have presented results on the behaviour of pulses in hydrodynamic jets. We found that high expansion speeds along the jet axis dominate the flow pattern. The lateral expansion and mass loss is relatively slow. A simple analytical model was developed in Section 3, based on one-dimensional hydrocode calculations (Sect. 2).

We are able to make various general predictions which relate jet dynamical properties to the observable parameters. In particular, we find the following for high Mach number isothermal flows.

(1) The number of evenly spaced knots and the number of knots in a jet before the knots lose their individual identities depend only on the jet Mach number (Sect. 6.1).

(2) The number of observable knots depends only (and inversely) on the pulse amplitude relative to the jet speed (Sect. 6.1).

(3) After a low-brightness gap, a second series of knots begins. The power radiated from these knots, and the degree of brightening, are related to those of the first series by a factor which depend solely on the pulse Mach number (Sect. 6.2)

(4) The knots will be extremely difficult to resolve spectroscopically since spectral widths only become large when the energy flux is small. However, one may also be able to observe the sawteeth themselves rather than the high density knots.

Can intermediate teeth be distinguished from other shock patterns? The tranverse shocks predicted here tend to lead to lead to isolated clumps. Fluid-dynamic instabilities produce twisted and filamentary structures and oblique shocks (Hardee & Clarke 1992). Pinching modes of the Kelvin-Helmholtz instability may, however, also produce a series of knots. The important prediction here is that pulses tire very rapidly (e.g. see Suttner et al

1996) whereas instabilities, at worst, will saturate rather than damp.

The frequency of the initial perturbations and the jet speed will determine the knot spacing. The amplitude of the perturbation and the jet Mach number will determine the other jet properties. The frequency is perhaps the most interesting quantity, placing constraints on accretion instabilities or stellar wind pulsations. The pulse amplitude, however, can also provide information about the flow origin. Small amplitude perturbations, for example, suggest that no explosive FUor type outburst is responsible. The appearance of numerous knots, such as observed at the base of the HH 111 jet (Reipurth et al 1992), is then predicted. In HH 111 there is some evidence for a low amplitude sawtooth structure with individual Hα emission-line components corresponding to the individual shocks rather than complete knots. Spectroscopy is required, however, to determine the underlying fluid speeds.

Ideally, pulses could be confirmed through slit-spectroscopy across an intermediate tooth in a stellar jet. This is presently practical, given the above formula for observable knot sizes, provided the pulse Mach number is not too large. For example a pulse wavelength of 310^{17} cm and Mach number of 4, corresponding to shocks of $40\,\mathrm{km\,s^{-1}}$ in an atomic jet, yield an observable knot (by the definition in Sect. 6.2) of width 9 arcseconds at 140 parsecs. However, the implied Mach number for a hydrodynamic molecular jet is ~ 100 which yields very small knot widths of < 0.03 arcseconds. These results are relevant to forthcoming observations of protostellar jets in the infrared. The detailed spatial and velocity structure of individual bright knots which initiate some jets may reveal the full pulse structure. Examples are found in the outflows of HH212 (Zinnecker et al 1996), HH1/2, HH30, HH46/47 and HH111 (see Ray (1996)). Theoretically, having established the general properties, it will now be possible to study the influence of chemical and physical processes and the peculiarities of specific flow patterns. In one such study, Suttner et al (1996) show that molecule dissociation in the shocks produces more complex teeth. A second study (Mac Low & Smith 1996) will help us to identify magnetohydrodynamic cushioning and ambipolar diffusion within jets.

Acknowledgements. We sincerely thank H. Yorke, F. Schmitz and the referee. We also thank the DFG for financial support.

References

Bahcall, J., et al 1995, ApJL, 452, L91.
Biro, S., Raga, A., 1994, ApJ, 434, 221
Eislöffel, J., Mundt, R., 1994, A&A, 284, 530
Falle, S.A.E.G., Raga, A.C. 1993, MNRAS, 261, 573
Ferrari, A., Trussoni, E. & Zaninetti, L., A&A, 125, 179
Hardee, P.E. & Clarke, D.A., ApJL, 400, L9
Hartigan, P. Raymond, J. 1993, ApJ, 409, 705
Loken, C.,Burns, J.O., Norman,M.L. & Clarke, D.A., 1993, ApJ, 417, 515
Mac Low, M., Smith, M.D. 1996. In preparation.
Etad, E. 1994, in Instrumentation in Astronomy VIII, SPIE v2198, in press
Raga, A.C., Cantó, J., Binette, L., Calvet, N., 1990, ApJ, 363, 601
Raga, A.C., Cantó, J., Calvet, N., Rodríguez, L.F., Torrelles, J.M., 1993, A&A 276, 539
Raga, A.C. & Kofman, L. 1992, ApJ, 386, 222
Ray, T.P. 1996,, in Solar and Astrophysical MHD Flows, ed K. Tsinganos, Astrophys. Lett. & Comm. (Kluwer).
Reipurth, B., Raga, A.C., Heathcote, S. 1992, ApJ, 392, 145
Stone, J.M. & Norman, M.L. 1992, ApJS, 80, 753.
Stone, J.M. & Norman, M.L. 1993, ApJ, 413, 210
Suttner, G., Smith, M.D., Yorke, H., Zinnecker, H. 1996, A&A submitted.
Ziegler, U., Yorke, H., Kaisig, M., 1996, A&A, 305, 114.
Zinnecker, H. et al 1996, in preparation.

This article was processed by the author using Springer-Verlag LaTeX A&A style file *L-AA* version 3.